High-field magnetoresistance and de Haas–van Alphen effect in antiferromagnetic PrB_6 and NdB_6

Y. Onuki,* A. Umezawa,† W. K. Kwok,‡ and G. W. Crabtree
Material Science Division, Argonne National Laboratory, Argonne, Illinois 60439

M. Nishihara, T. Yamazaki, T. Omi, and T. Komatsubara
Institute of Material Science, University of Tsukuba, Sakura-mura, Ibaraki 305, Japan
(Received 17 July 1989)

The transport properties and the de Haas–van Alphen (dHvA) effect have been measured for antiferromagnetic PrB_6 and NdB_6. The number of conduction electrons is approximately one per unit cell. The magnetoresistance shows the existence of open orbits, implying a multiply connected Fermi surface. The angular dependence of the magnetoresistance is roughly similar to that of the reference material, LaB_6. The dHvA data in PrB_6 show both paramagnetic and antiferromagnetic Fermi surfaces. The antiferromagnetic Fermi surface arises from new magnetic Brillouin zone boundaries and antiferromagnetic gaps introduced by the magnetic order, and the paramagnetic Fermi surface from magnetic breakdown through the small antiferromagnetic gaps in high field. Hybridization between the conduction electrons and the f electrons has been observed through the cyclotron masses, which in PrB_6 are three times larger than the corresponding masses of LaB_6. In NdB_6 only the antiferromagnetic Fermi surface, quite different from those of LaB_6 and PrB_6, has been observed.

I. INTRODUCTION

In many rare-earth and actinide compounds the f electrons show a wide variety of behavior, including Pauli itinerance, spin fluctuations, mixed valence and heavy fermions, and local moment magnetic order.[1–3] The rare-earth hexaborides RB_6 are an interesting series of compounds where systematic f-electron behavior including many of these features can be studied. LaB_6 is a non-f-electron transition-metal-like system, CeB_6 is a typical Kondo substance, PrB_6 and NdB_6 are local moment metals, and SmB_6 is a mixed valence compound with a gap in the narrow $4f$ band just at the Fermi level. Many experimental and theoretical studies are focused on the peculiar $4f$ behavior of these substances.

If the $4f$ electrons are completely localized, R^{3+}, there is no hybridization between the $4f$ electrons and the conduction electrons. The Fermi surface and cyclotron mass are almost the same as those of the non-f La compounds. In this case the $4f$ electrons act only as scattering centers for the conduction electrons. However, as the $4f$ states approach the Fermi level in energy in going from Gd to Ce, the f electrons hybridize more strongly with the conduction electrons. The most highly hybridized state is expected in the Ce compound. In RB_6 the Ce compound displays a large electronic specific heat typical of f-electron hybridization, yet still retains a large enough moment to order magnetically at low temperature.[4–6] The reduced moment and logarithmic-like resistivity in CeB_6 are typical of the Kondo effect.

In general, the Ruderman-Kittel-Kasuya-Yosida (RKKY) interaction competes with the Kondo effect by creating an exchange coupling between f moments, which leads to magnetic order at low temperatures. As the number of f electrons increases in the RB_6 series, the moment becomes larger and the RKKY interaction stronger, leading to magnetic-ordering temperatures which roughly follow the de Gennes relation. The antiferromagnetic-ordering temperatures in CeB_6, PrB_6, and NdB_6 are 2.4, 7.0, and 7.8 K, respectively,[4–7] in approximate agreement with the de Gennes relation.

The presence of the f electron in RB_6 alters the Fermi surface in three ways: through hybridization with the conduction electrons, through the f-electron contribution to the crystal potential, and through the introduction of new magnetic Brillouin zone boundaries and magnetic energy gaps which occur when the f-electron moments order. The first two mechanisms alter the electronic band structure of the metal and may affect both the Fermi-surface geometry and cyclotron effective masses. The two mechanisms are difficult to separate from each other, although some separation can be achieved[8] by careful Fermi-surface measurements and band-structure calculations. The effect of the third mechanism can be approximated by a band-folding procedure where the paramagnetic Fermi surface containing all the corrections due to hybridization and crystal potential effects is folded into the smaller Brillouin zone induced by the antiferromagnetic order. If the magnetic energy gaps associated with the antiferromagnetic structure are small enough, electrons undergoing cyclotron motion in the presence of a magnetic field can tunnel through these gaps and follow orbits on the paramagnetic Fermi surface. If this magnetic breakdown occurs, the paramagnetic Fermi surface may be observed in the de Haas–van Alphen (dHvA) effect even in the presence of magnetic

order. However, if there is significant hybridization or a large contribution of the f electron to the crystal potential, the paramagnetic Fermi-surface may be somewhat different from the non-f analog metal. Generally, one expects hybridization to appear in the dHvA results as an increased cyclotron effective mass due to the admixture of the heavier and highly correlated f electrons with the spd conduction electrons. Such effects have been observed[9–11] in $CeSn_3$, $CeCu_6$, and UPt_3.

The first investigations of the Fermi surfaces of the RB_6 compounds were done on LaB_6 by Arko *et al.*[12,13] using magnetoresistance and the dHvA effect in fields up to 13.2 T and temperature down to 0.35 K and by Ishizawa *et al.*[14,15] using the dhvA effect in fields up to 6 T and at temperatures as low as 1.5 K. The experimental results were interpreted by a Fermi-surface model consisting of large electron sheets at the X point of the Brillouin zone connected by tiny necks in the X-X direction as illustrated in Fig. 1. Band-structure calculations carried out by Walch *et al.*[16] and by Hasegawa and Yanase[17] confirmed the general topology of the empirical Fermi-surface model but were unable to provide a quantitative explanation of all the observed orbits. However, the geometry of the electron sheets at X which contain nearly all the electrons and determine the electronic behavior were qualitatively well explained.

Systematic Fermi-surface measurements on LaB_6, CeB_6, PrB_6, and NdB_6 were first carried out by van Deursen *et al.*[18] for the single field direction ⟨100⟩ using pulsed fields up to 33 T at temperatures down to 1.3 K. They observed one frequency in CeB_6 and up to five frequencies in the other compounds which suggested the Fermi-surface topology for all the compounds was similar. Later work[19] on the anisotropy of the frequencies in CeB_6 and PrB_6 confirmed the existence of the X-centered ellipsoids in PrB_6 and revealed some additional features not directly analogous to LaB_6 which suggested the existence of smaller closed sheets.

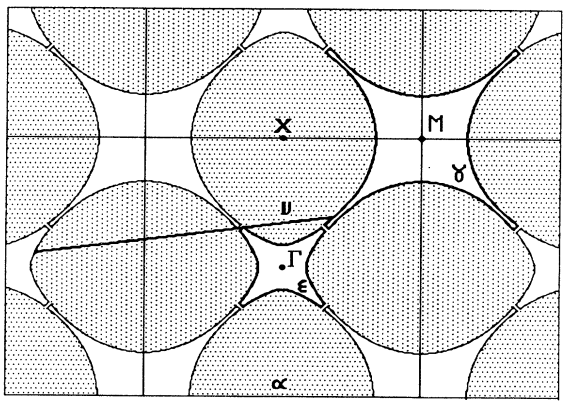

FIG. 1. Cross section of the LaB_6 Fermi surface in the ΓXM plane. Lower case Greek letters α γ, ϵ, and ν refer to particular orbits on the surface.

An independent study of the Fermi surface of PrB_6 using the dHvA effect and magnetoresistance in fields of 15 T at temperatures down to 1.4 K by Onuki *et al.*[20] provided a more complete picture of the Fermi-surface geometry and effective masses in PrB_6. This work revealed two sets of low-frequency orbits with the same anisotropy as those arising from the X-X neck orbits in LaB_6 but with areas approximately 100 times and 30 times larger than those in LaB_6. This more extensive data generally agreed with those of van Deursen *et al.* for the areas and masses where comparison was possible.

In this paper we continue investigations of the Fermi-surface properties of the RB_6 series with magnetoresistance and Hall-effect measurements in CeB_6, PrB_6, and NdB_6 and with additional dHvA measurements in NdB_6 in fields up to 15 T and temperatures down to 0.4 K. In CeB_6 we find features characteristic of the Kondo effect. In PrB_6 we present new data on the open orbits from the magnetoresistance. In NdB_6 we present for the first time the detailed variation of the dHvA frequencies and effective masses with magnetic field direction. We compare our data for all three rare-earth compounds with those of LaB_6 and discuss the implications for models of the f-electron behavior.

II. EXPERIMENTAL PROCEDURES

Single crystals of RB_6 were grown by a floating-zone technique. Three passes of the molten zone were made on each crystal in an atmosphere of Ar at 30 bar to prevent excessive evaporation. The typical dimensions of the resulting crystalline bars were 8 mm in diameter and 40 mm in length.

The electrical resistivity, magnetoresistance, and Hall coefficient were measured by a dc method. The Hall coefficient was measured in the temperature range of 0.7 K to room temperature in a field of 0.8 T, where the Hall voltage was linear in the field. The magnetoresistance was measured at 1.4 K in fields up to 15 T. The dHvA experiments were carried out at 0.4 K in fields up to 15 T using field modulation and second-harmonic detection. The dHvA frequencies were obtained by taking fast Fourier transforms of the oscillatory magnetization signal. Effective masses were determined from the temperature dependence of the amplitude of the signal at fixed field.

III. EXPERIMENTAL RESULTS AND ANALYSIS

The temperature dependence of the electrical resistivity of single-crystal samples of RB_6 for the current along the ⟨100⟩ direction is shown in Fig. 2. The residual resistivity ratio $\rho_{RT}/\rho_{1.4\,K}$ is 220 in PrB_6 and 120 in NdB_6. The inset shows the steep decrease of the resistivity below 7.0 K in PrB_6 and 7.8 K in NdB_6 which is due to antiferromagnetic ordering in these compounds.[6,7] Two steps at 7.0 and 4.2 K in PrB_6 correspond to the appearance of incommensurate and commensurate spin structures, respectively. The resistivity of CeB_6 shows a dense Kondo behavior, increasing logarithmically with decreasing temperature until it passes through a maximum at 4.0

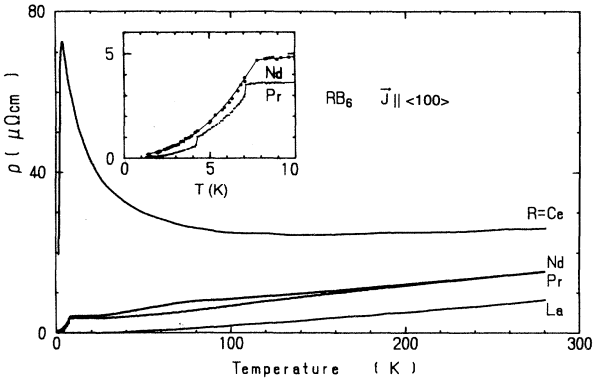

FIG. 2. Temperature dependence of the electrical resistivity in RB_6.

K and decreases quite rapidly at lower temperatures. CeB_6 undergoes two ordering transitions at 3.2 and 2.3 K, where the lower one is due to the onset of antiferromagnetic order.[4,5,21,22]

The temperature dependence of the Hall coefficient in single crystal RB_6 is shown in Fig. 3. The Hall coefficient is almost temperature independent, except for the region near the ordering temperature of CeB_6. The present results are $-(4.5\pm0.7)\times10^{-4}$ cm^3/C in CeB_6, $-(3.9\pm1.1)\times10^{-4}$ cm^3/C in PrB_6, and $-(4.6\pm0.9)\times10^{-4}$ cm^3/C in NdB_6. The Hall coefficient of LaB_6 was measured by Tanaka *et al.*[23] to be -4.5×10^{-4} cm^3/C. Using the lattice constants of RB_6 (R :La, 4.156 Å; Ce, 4.140 Å; Pr, 4.133 Å; and Nd, 4.126 Å) we calculate the number of conduction electron per unit cell to be 1.0, 1.0±0.1, 1.2±0.3, and 1.0±0.2, respectively. These

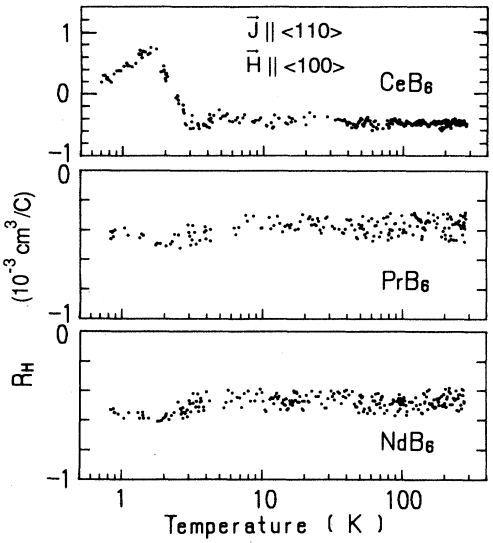

FIG. 3. Temperature dependence of the Hall coefficient in RB_6.

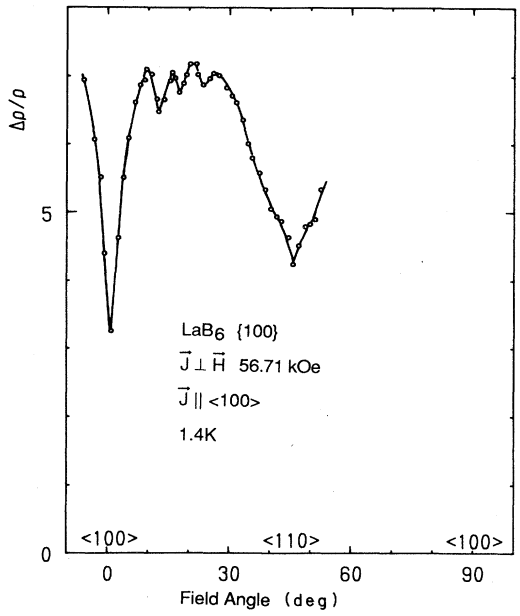

FIG. 4. Angular dependence of the transverse magnetoresistance of LaB_6 in the {100} plane. Data are taken from Ref. 24.

values of the electron densities are consistent with the Fermi surface of LaB_6, which fills half the Brillouin zone with the three nearly spherical ellipsoids at X. Band calculations of LaB_6 show that the electron states at the Fermi surface are mainly of 5*d*-character implying that they originate from the rare-earth atom.

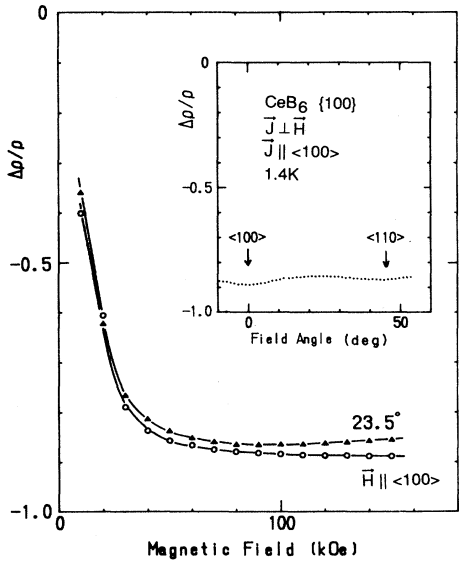

FIG. 5. Angular dependence of the transverse magnetoresistance of CeB_6 in the {100} plane.

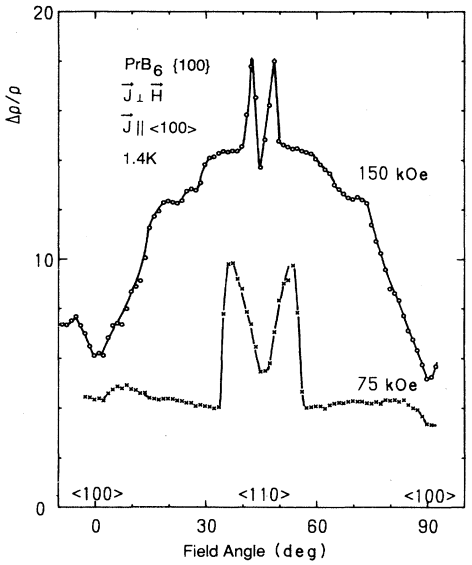

FIG. 6. Angular dependence of the transverse magnetoresistance of PrB_6 in the {100} plane.

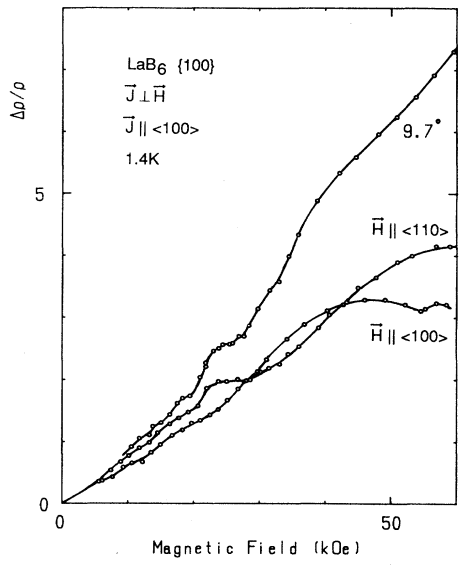

FIG. 8. Field dependence of the transverse magnetoresistance of LaB_6 at typical field directions in the {100} plane. The data are taken from Ref. 24.

We show in Figs. 4–7 the angular dependence of the transverse magnetoresistance $\Delta\rho/\rho=[\rho(H)-\rho(0)]/\rho(0)$ of RB_6 in the {100} plane, and in Figs. 8–10 the field dependence of the transverse magnetoresistance in selected field directions. The data of LaB_6 have been taken from Ref. 24. When the field is applied along the ⟨100⟩ direction, the magnetoresistance saturates at high fields in LaB_6, PrB_6, and NdB_6. Nonsaturating behavior is observed in all other directions in the {100} plane. For uncompensated metals like LaB_6, this behavior is characteristic of the existence of an open orbit along the ⟨100⟩ current direction.

We have observed a complicated behavior in the magnetoresistance of PrB_6. The magnetoresistance saturates above 100 kOe for fields directions between about 5–40°, and 55–85° from ⟨100⟩. This behavior is due to magnetic breakdown effects resulting in topological changes of

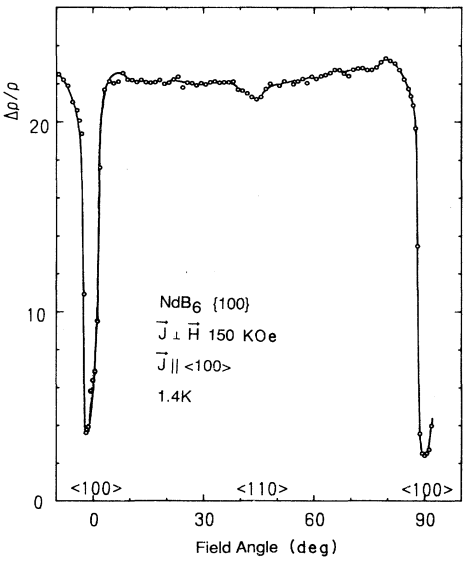

FIG. 7. Angular dependence of the transverse magnetoresistance of NdB_6 in the {100} plane.

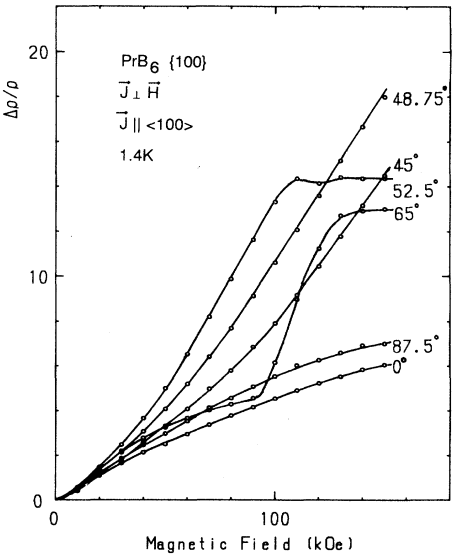

FIG. 9. Field dependence of the transverse magnetoresistance of PrB_6 at typical field directions in the {100} plane.

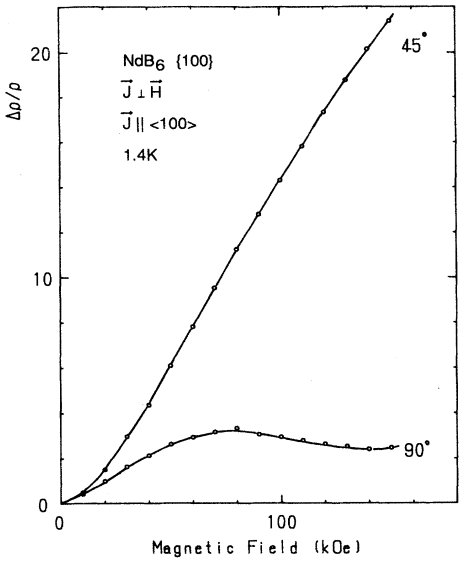

FIG. 10. Field dependence of the transverse magnetoresistance of NdB_6 at typical field directions in the {100} plane.

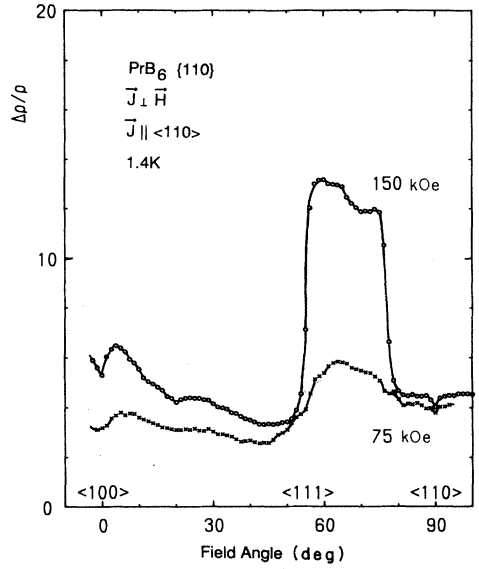

FIG. 12. Angular dependence of the transverse magnetoresistance of PrB_6 in the {110} plane.

the orbit and is not found in NdB_6. The oscillatory magnetoresistance in LaB_6 is due to Shubnikov–de Haas oscillations on the small neck connecting the X-centered ellipsoids. We note that both PrB_6 and NdB_6 are in the antiferromagnetic phase for the fields and temperatures employed in the magnetoresistance experiments. Our preliminary magnetization measurements show that this antiferromagnetic phase is stable up to at least 400 kOe. We also stress that the magnitude of $\Delta\rho/\rho \sim 20$ at 150 kOe in the open orbit direction is consistent with the high-field condition $\omega_c\tau > 1$ because the relationship $\Delta\rho/\rho = (\omega_c\tau)^2$ approximately holds for the nonsaturating magnetoresistance. Here, ω_c is the cyclotron frequency and τ is the relaxation time of the carrier. The value of $\omega_c\tau$ is the number of the cyclotron orbits completed between scattering events.

The magnetoresistance of CeB_6 is negative, which is characteristic to the Kondo effect. In the low-field region

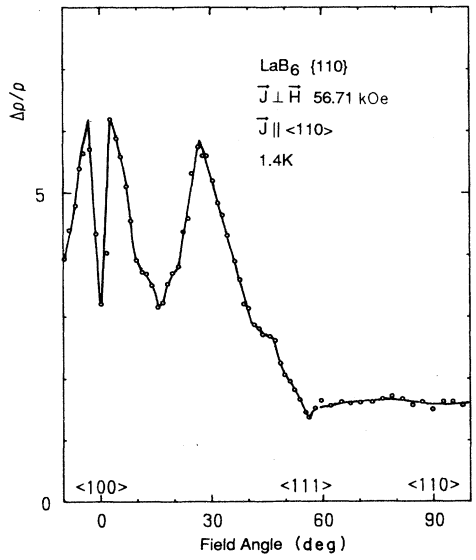

FIG. 11. Angular dependence of the transverse magnetoresistance of LaB_6 in the {110} plane. The data were taken from Ref. 24.

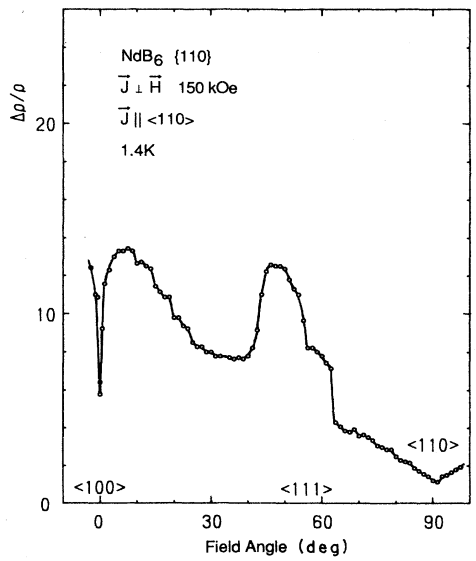

FIG. 13. Angular dependence of the transverse magnetoresistance of NdB_6 in the {110} plane.

TABLE I. Field directions at which open orbits are observed in LaB_6, PrB_6, and NdB_6. The data of LaB_6 was taken from Ref. 24.

	Angle from the ⟨100⟩ direction in the {100} plane	Angle from the ⟨100⟩ direction in the {110} plane
LaB_6	Whole region except the ⟨100⟩ direction	1–10° 10–35°
PrB_6	Whole region except the ⟨100⟩ direction	55–77°
NdB_6	Whole region except the ⟨100⟩ direction	1–24° 42–55°

the negative magnetoresistance is related to magnetization M by $\Delta\rho/\rho \propto -M^2$. At high fields above 100 kOe, the magnetoresistance in the field direction of 23.5° increases slightly with field. We suppose that the positive magnetoresistance due to the cyclotron motion of the carriers is added to the negative magnetoresistance mentioned above. The magnetoresistance is known to become positive[25] at 0.5 K above 50 kOe. Apparently at high enough field and low enough temperature, the magnetization-dependent negative magnetoresistance saturates, leaving the positive magnetoresistance due to Fermi-surface effects. In this low-temperature high-field region topological information on the Fermi surface of CeB_6 could be determined.

The angular dependences of the transverse magnetoresistance of RB_6 in the {110} plane are shown in Figs. 11–13, while the field dependences are shown in Figs. 14–16. Nonsaturating behavior due to the existence of open orbits is found in the region of 1–10° and 20–35° from ⟨100⟩ in LaB_6. Similar behavior is observed in NdB_6 in the region of 1–24° and 42–55° from ⟨100⟩. PrB_6 does not show such nonsaturating behavior in the vicinity of the ⟨100⟩ direction. The nonsaturating behavior is only found in the region of 55–77° from ⟨100⟩. Although the ⟨100⟩ direction is the so-called singular field direction in LaB_6 and NdB_6, it is not so in PrB_6.

We summarize the open orbit directions derived from the magnetoresistance data in Table I. The existence of open orbits confirms the multiply connected nature of the Fermi surface and can be understood qualitatively on the basis of the Fermi-surface model of Fig. 1 as explained further below.

Finally, we show in Figs. 17–19 the angular dependence of dHvA frequencies in RB_6. The data of LaB_6 has been taken from Refs. 14 and 15. The ⟨100⟩ frequencies and the corresponding cyclotron masses which have been determined from the temperature dependence of the dHvA oscillations are tabulated in Table II.

Although there is a great deal of detailed data concerning the Fermi surfaces of the RB_6 compounds in Figs. 17–19, there are some systematic features which can be qualitatively understood with a simple picture. We note that there are many similarities in the dHvA data of LaB_6

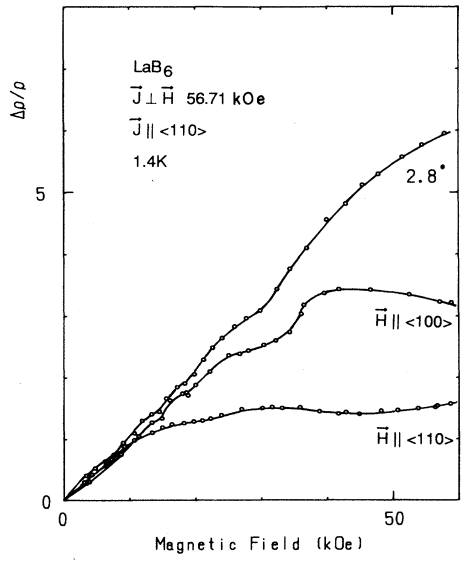

FIG. 14. Field dependence of the transverse magnetoresistance of LaB_6 at typical directions in the {110} plane. The data were taken from Ref. 24.

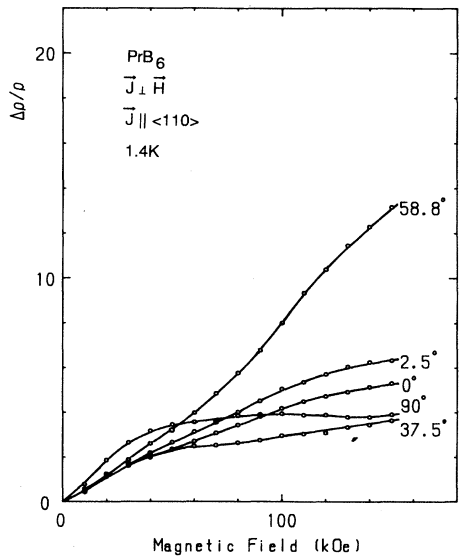

FIG. 15. Field dependence of the transverse magnetoresistance of PrB_6 at typical directions in the {110} plane.

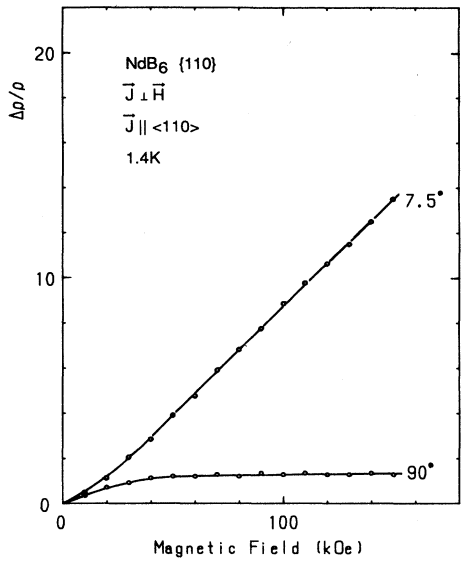

FIG. 16. Field dependence of the transverse magnetoresistance of NdB_6 at typical directions in the {110} plane.

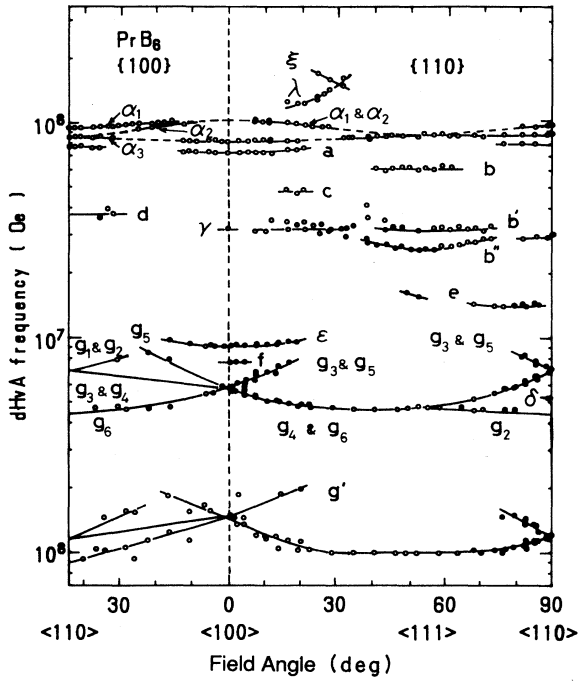

FIG. 18. Angular dependence of the dHvA frequencies in PrB_6.

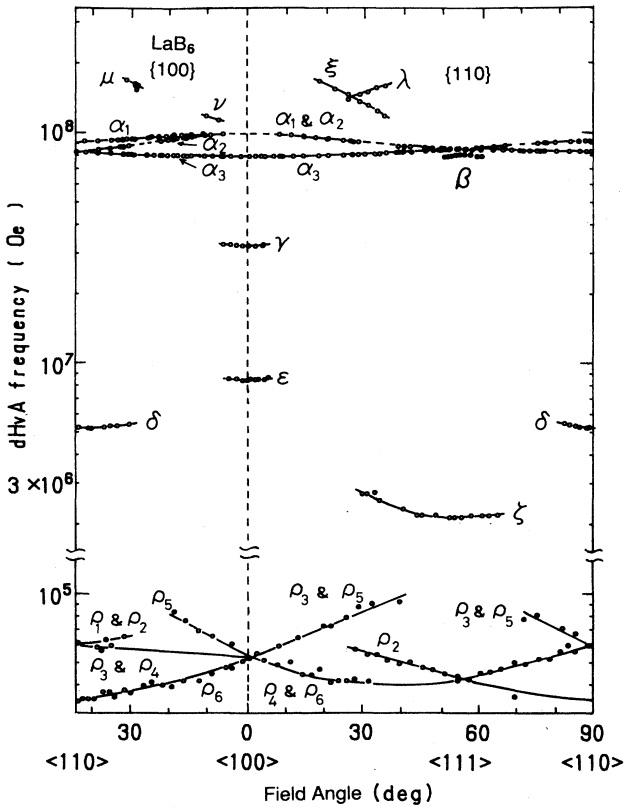

FIG. 17. Angular dependence of the dHvA frequencies in LaB_6. The data were taken from Refs. 14 and 15.

and PrB_6, but almost no similarity between the data in Lab_6 and those in NdB_6. Close examination reveals that the α, γ, ϵ, δ, γ, and ξ branches in LaB_6 correspond in angular dependence and magnitude approximately with

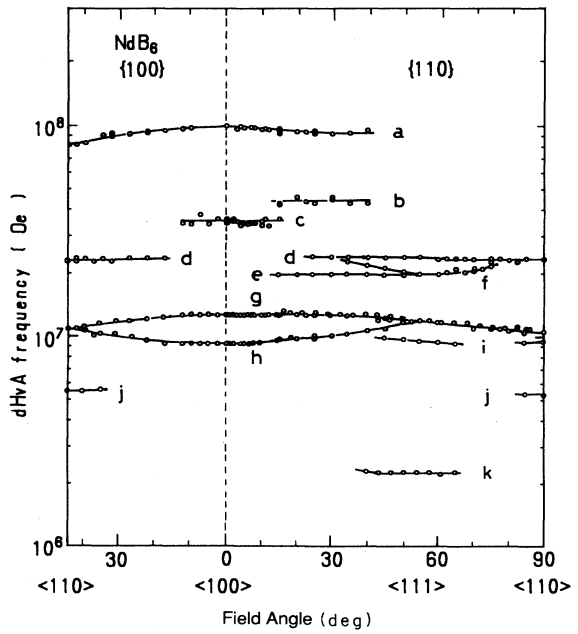

FIG. 19. Angular dependence of the dHvA frequencies in NdB_6.

branches in PrB_6. These branches have been so labeled in the data for PrB_6 in Fig. 18. The other branches in PrB_6 which do not correspond to branches in LaB_6 have been labeled with Arabic letters. The α frequency in PrB_6 has three branches α_1, α_2, and α_3 in the $\{100\}$ plane, and it degenerates into two in the $\{110\}$ plane, as is observed in LaB_6. The cyclotron mass of the α_3 orbit in PrB_6, $1.95m_0$, is three times larger than the corresponding mass in LaB_6, 0.61–$0.64m_0$. Except for the ρ and ξ oscillations, all of the long-range frequencies in LaB_6 are also observed in PrB_6.

The g and g' branches in PrB_6 are very similar in shape to the ρ branches in LaB_6 but are much larger in magnitude. The dHvA frequencies of g and g' in the $\langle 100 \rangle$ direction are 5.9×10^6 Oe and 1.5×10^6 Oe, respectively, which are 130 times larger than 5.2×10^4 Oe as observed in LaB_6. The masses on these orbits are $0.62m_0$ and $0.28m_0$, heavier than the corresponding value $0.046m_0$ in LaB_6. In LaB_6 these branches arise from the necks which connect the X-centered ellipsoids. We propose that a similar feature exists in PrB_6, except that there are two necks connecting each ellipsoid and the necks are appropriately larger.[20]

The similarity of the Fermi surfaces of LaB_6 and PrB_6 is surprising because PrB_6 orders with a complicated magnetic structure involving 32 units cells.[6] This introduces a magnetic Brillouin zone which is much smaller than the X-centered ellipsoids. When the Fermi surface is folded into the new Brillouin zone, the large orbits such as α are interrupted by zone boundaries and should not appear in the data. We explain the similarity of the dHvA data in LaB_6 and PrB_6 by magnetic breakdown, assuming the applied field is strong enough to drive the electrons through the energy gaps created at the magnetic Brillouin zone boundaries by the antiferromagnetic structure. In that case the paramagnetic Fermi surface would be observed, and it may be similar to that of LaB_6 if the effects of hybridization and the f-electron crystal potential are not too large.

The branches in PrB_6 that are not observed in LaB_6 we attribute to the antiferromagnetic Fermi surface. These branches represent the paramagnetic Fermi surface folded into the smaller magnetic Brillouin zone. With incomplete magnetic breakdown both the paramagnetic and antiferromagnetic Fermi surfaces can be seen. The a branch is the largest frequency on the antiferromagnetic

TABLE II. dHvA frequencies and cyclotron masses in LaB_6, PrB_6, and NdB_6 for the field along the $\langle 100 \rangle$ direction. Data by Ishizawa *et al.*, Arko *et al.*, and van Deursen *et al.* are from Refs. 14 and 15, 12 and 13, and 18 and 19, respectively.

			LaB_6			
	Ishizawa *et al.*		Arko *et al.*		van Deursen *et al.*	
	$F(\times10^7$ Oe)	m^*/m_0	$F(\times10^7$ Oe)	m^*/m_0	$F(\times10^7$ Oe)	m^*/m_0
α_1 and α_2			10.09		10.03	0.7±0.1
α_3	7.89	0.64	7.89	0.61	7.89	0.6±0.1
γ	3.22		3.22		3.24	
ϵ	0.85		0.86		0.83	
ρ	0.0052	0.046				

			PrB_6	
	Present results		van Deursen *et al.*	
	$F(\times10^7$ Oe)	m^*/m_0	$F(\times10^7$ Oe)	m^*/m_0
α_1 and α_2			10.14	2.1±0.2
α_3	8.19	1.95	8.09	1.6±0.2
γ	3.27	1.94	3.23	1.6±0.2
ϵ	0.94	0.94	0.94	1.1±0.2
a	7.25	2.52	7.2	
f	0.79	0.66	0.82	
g	0.59	0.62	0.58	
g'	0.15	0.28		

			NdB_6	
	Present results		van Deursen *et al.*	
	$F(\times10^7$ Oe)	m^*/m_0	$F(\times10^7$ Oe)	m^*/m_0
α_3			7.98	0.6±0.2
a	9.90	2.00		
c	3.44	2.43	3.39	
g	1.27	1.47	1.21	
h	0.95	1.08	0.92	1.0±0.2

Fermi surface. This signal disappears in the field range of 13–35° from ⟨100⟩ in the {100} plane and 22–77° from ⟨100⟩ in the {110} plane. The Fermi-surface sheet giving rise to the a orbit is nearly spherical, being slightly stretched in the ⟨100⟩ direction and may possess arms which cause the orbit to disappear. These arms are probably in the ⟨111⟩ direction.

Besides the a, g, and g' branches, three branches b, b', and b'' are observed, centered at the ⟨111⟩ direction. van Deursen *et al.*[19] observed another similar branch with a frequency of 3.7×10^7 Oe in the ⟨111⟩ direction.

The dHvA frequencies observed in NdB_6 are extremely different from those of LaB_6 and PrB_6. In fact, there are no oscillations which correspond to those of LaB_6. The characteristic features in the Fermi surface of NdB_6 are as follows. The a branch is a nearly spherical Fermi surface which is slightly stretched in the ⟨100⟩ direction. The signal of the a branch, however, disappears in the field angle of 40–90° from ⟨100⟩ in the {110} plane. Moreover, it becomes extremely weak in the vicinity of the ⟨100⟩ direction, possessing a maximum amplitude at about 10°.

The g and h branches are nearly spherical ellipsoids. As there is no third branch in the {100} plane, g and h may not be symmetry equivalent ellipsoids. The signal of the h branch seems to be degenerate with the g signal in the field range of 55° to 90°. We do not believe that the h signal simply disappears for angles greater than 55°, because its amplitude is quite strong for directions near ⟨111⟩.

The other branches are limited to small angle regions. The c branch possesses a symmetry at the ⟨110⟩ direction, the d and j branches at the ⟨110⟩ direction, and the f and k branches at the ⟨111⟩ direction.

IV. DISCUSSION

The data presented above can be understood using simple ideas for the effect of the f electron on the Fermi surface through the crystal potential, hybridization, and magnetic order. We argue that the main features of the paramagnetic Fermi surfaces of LaB_6, PrB_6, and NdB_6 are all similar, with large ellipsoids at X connected by necks in the X-X directions. Slight differences in the band structures of the three metals due to the contribution of the f electron to the crystal potential or to direct hybridization of the conduction states with the f electron alter details of the Fermi-surface geometry like the shape of the ellipsoids and the size and connectivity of the necks. If significant f-electron hybridization occurs, the effective masses of the paramagnetic Fermi surface are increased relative to LaB_6. When magnetic order occurs, the paramagnetic Fermi surface must be folded into the smaller magnetic Brillouin zone, perhaps altering the observable cyclotron orbits drastically. However, if the magnetic energy gaps at the new zone boundaries are not too large, the paramagnetic Fermi surface can still be seen due to magnetic breakdown. If the applied field range spans the breakdown field, the paramagnetic and antiferromagnetic Fermi surfaces will be seen simultaneously. This case applies to PrB_6. If the magnetic energy gaps are too large, the breakdown field will be large compared to the applied field and no magnetic breakdown will occur. In this case only the antiferromagnetic Fermi surface will be seen, as occurs in NdB_6.

First we justify the claim that the main features of the paramagnetic Fermi surfaces of LaB_6, PrB_6, and NdB_6 are essentially the same. There are three reasons for this assertion. First, the value of the Hall coefficient in RB_6 is almost the same at room temperature in all three compounds. The number of conduction electrons is approximately one per unit cell, suggesting that all three metals have the ellipsoidal X-centered surfaces of LaB_6. Even below the Néel temperature, the carrier concentration does not change in PrB_6 and NdB_6 as indicated by the temperature independence of the Hall coefficient, an unusual feature in magnetically ordered metals. Secondly, the Fermi surface determined by two-dimensional angular correlation of positron annihilation radiation shows nearly the same shape for all RB_6 compounds at room temperature.[26] The positron annihilation results show directly the existence of an electron ellipsoid at the X point. This work confirms the interpretation of the Fermi surface discussed above. Finally, we observe the α orbits arising from the X-centered ellipsoids in both LaB_6 and PrB_6, but not in NdB_6. However, as shown in Table II, van Deursen *et al.*[18] observed four dHvA signals in the ⟨100⟩ field direction in NdB_6. Three of them correspond to the c, g, and h branches in the present experiment. The other dHvA frequency in 7.98×10^7 Oe, which corresponds to the α_3 branch of the X-centered ellipsoid. Their observation of this magnetic breakdown orbit in NdB_6 is due to their use of high fields of 29 T compared to our highest field of 15 T. Thus the basic feature of the LaB_6 Fermi surface is seen by dHvA measurements in both PrB_6 and NdB_6. Based on the Hall coefficient data, the positron annihilation data, and the high-field dHvA data, we conclude that the paramagnetic Fermi surfaces of all three metals are very similar.

Despite the basic similarity in the main features of the paramagnetic Fermi surfaces of LaB_6, PrB_6, and NdB_6 there are small differences in the details of the geometry related to the size and connectivity of the necks. These differences can be seen in the open orbit behavior derived from the magnetoresistance data and in the dHvA data.

First we discuss the magnetoresistance. The magnetoresistance of NdB_6 in fields up to 15 T is very similar to that of LaB_6. The analogous features are as follows: (1) The ⟨100⟩ direction is the singular field direction. (2) The open orbit in the {100} plane is found in all field directions except the ⟨100⟩ direction. (3) Open orbits of NdB_6 in the {100} plane exist in the range of 1–24° and 41–55°, while the one of LaB_6 exists in the range of 1–10° and 20–35°.

In PrB_6, open orbits are observed in the whole region of the {100} plane except the ⟨100⟩ direction and its vicinity. Unlike in LaB_6 and NdB_6, ⟨100⟩ is not a singular direction because there is a finite range of angles near ⟨100⟩ in which no open orbit is found. In the {100} plane open orbits are found in only one angular range,

55–77° from ⟨100⟩, instead of two ranges as in LaB_6 and NdB_6.

The angles at which the open orbits appear and disappear provide information about the placement and size of the necks in the paramagnetic Fermi surface. The open orbits on the LaB_6 Fermi surface for various field directions are shown in Fig. 20. For the field near the ⟨100⟩ direction in the {110} plane [Fig. 20(b)] the open orbit trajectory runs between two necks in the region labeled "*A*." The angular region of the open orbit is restricted by the existence of these two necks. If the Fermi surface of PrB_6 is similar to that of LaB_6, we infer that the two necks mentioned above are so large that they approximately touch each other, explaining the absence of the open orbit near the ⟨100⟩ direction in the {100} plane in PrB_6. The trajectory of the open orbit shown in Fig. 20(c) is also restricted by two necks, namely, one neck which the orbit must avoid near the *B* point and a second neck which is part of the orbit at the *C* point [the *C* neck is hidden by an ellipsoid in the view of Fig. 20(a)]. If the neck is small, this open orbit will be found at angles close to ⟨100⟩. In LaB_6, the open orbit first appears at 20° from ⟨100⟩ in the {110} plane. As the field angle becomes larger than 20°, the path gradually deviates from the *C* neck eventually forming a closed orbit at approximately 35°. In PrB_6, the neck is expected to be relatively large, as confirmed by the appearance of the open orbit at the rather high angle of 55° from ⟨100⟩ in the {110} plane.

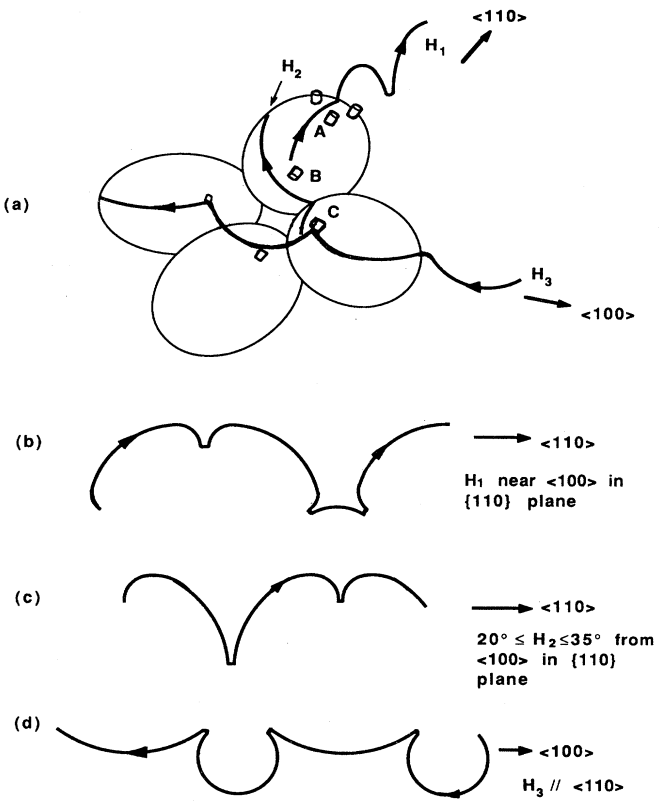

FIG. 20. Trajectories of the open orbits in LaB_6. The trajectories are labeled by the field directions shown in the figure, and the arrows show the open orbit directions.

This larger neck in PrB_6 is roughly consistent with the dHvA results. The α oscillation of PrB_6 disappears over a wider field range than in LaB_6, as shown in Table III, suggesting a larger neck dimension. As discussed in an earlier paper, such a result favors two interconnecting necks whose dimensions are roughly consistent with the g and g' orbit.[20] However, the length of the necks is very short if the ellipsoid dimensions of PrB_6 are the same as those of LaB_6. In this case we could not observe the g and g' oscillations over a wide field range or, in particular, for the field along the ⟨100⟩ direction. Therefore if the g and g' branches correspond to the necks in the paramagnetic Fermi surface, it is necessary to modify the shape of the ellipsoids in PrB_6.

If the above analysis is also applied to NdB_6, the neck of NdB_6 is a little larger than that of LaB_6 because the open orbit appears at 42° in the {110} plane. This cannot be confirmed with the dHvA results because only the antiferromagnetic Fermi surface is observed.

The magnetic breakdown phenomena that we invoke to explain the observation of the paramagnetic Fermi surface in PrB_6 can be observed on the paramagnetic Fermi surface itself. For example, for the field in the ⟨100⟩ direction the closed $\alpha 1$ $o\rho\beta\iota\tau$ in PrB_6 and LaB_6 should not exist because it is interrupted by a neck. However, as shown in Table II, at sufficiently high fields the α_1 orbit can be seen, implying magnetic breakdown across the neck, a feature that has been noted in earlier dHvA and band-structure studies of LaB_6. In the antiferromagnetic state the degree of magnetic breakdown through the magnetic zone boundary gaps depends on the size of the gaps. We expect these gaps to scale roughly with the magnitude of the magnetic moment or the de Gennes factor. Apparently the magnetic fields used in our experiment are large enough to cause magnetic breakdown through the gaps in PrB_6 but are too weak to cause breakdown in NdB_6.

Hybridization of the f electron with the conduction electrons can be seen most directly in the cyclotron effective masses. Because the f electrons are considerably more localized than the conduction electrons, hybridization with f electrons usually lowers the Fermi velocities and raises the effective masses of the hybridized state. Thus by comparing the effective masses of analogous orbits in RB_6, one infers the relative importance of hybirdization in the metals. On the paramagnetic Fermi surface of PrB_6 the mass of the α_3 orbit is $1.95m_0$, about three times larger than the mass of the corresponding orbit in LaB_6. This suggests that the $f$electron in PrB_6 is slightly hybridized with the conduction electrons. The increased mass in PrB_6 over LaB_6 is a general feature of the paramagnetic Fermi surfaces in the two materials as shown as shown in Fig. 21, where the mass versus frequency is plotted on a logarithmic scale. As shown, there is approximately a factor of 3 enhancement in all the

TABLE III. Angular ranges where the α oscillation is not observed in LaB_6 and PrB_6. The data of LaB_6 was cited from Ref. 14.

	LaB_6	PrB_6
{100}		
α_1	0–9°	0–15°
α_2	0–6° and 23–30°	0–12° and 26–40°
α_3		15–30°
{100}		
α_1	0–9° and 30–39°	0–5° and 30–40°
α_2		
α_3	68–75°	20–30° and 60–80°

measured masses in the two materials. If this enhancement is due to a narrowing of the bandwidth from f-electron hybridization, then Fig. 21 implies that the hybridization is approximately equally strong for all the conduction electrons in PrB_6. This general enhancement of all the masses when f-electron hybridization occurs has also been seen[9] in $CeSn_3$. The paramagnetic state of NdB_6, as measured by van Deursen *et al.* shows a return to the masses observed in LaB_6, suggesting that f hybridization is absent in this metal. This interpretation is consistent with the much larger binding energy of the f electron in Nd compared to Pr.

In the antiferromagnetic state, the Fermi surface changes due to the appearance of the magnetic zone boundaries can be approximated by folding the paramagnetic Fermi surface into the smaller magnetic Brillouin zone. The magnetic structure in RB_6 may be quite complicated even though its chemical structure is simple cubic. The magnetic unit cell of PrB_6 involves 32 formula units[6] and has a wave vector $\mathbf{q}=(0.25,0.25,0.5)\ 2\pi/a$, while in NdB_6 there is a simple doubling[7] of the chemical unit cell. We note that the reciprocal vector in the new magnetic unit cell of PrB_6 is not $(0.25,0.25,0.50)\ 2\pi/a$, but possesses the magnitude $[1/(2\sqrt{2})]\ 2\pi/a$ in the ⟨110⟩ direction. Earlier attempts to account for the experimental data of PrB_6 by folding the paramagnetic Fermi surface into the magnetic Brillouin zone were not successful. A quantitative procedure using an analytical model for the Fermi surface is required to explore this procedure.

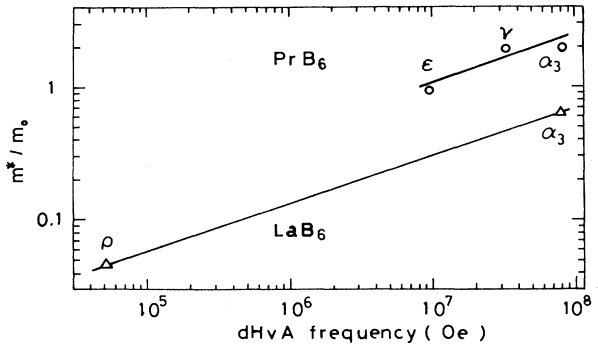

FIG. 21. Comparison of masses of LaB_6 and of the paramagnetic Fermi surface of PrB_6.

The dHvA frequencies and cyclotron masses in the antiferromagnetic state of PrB_6 and NdB_6 are highly different from those in the paramagnetic state. In PrB_6, the a branch is the highest frequency on the antiferromagnetic Fermi surface. This signal disappears in the angular region of 12–35° from ⟨100⟩ in the {100} plane and 20–75° from ⟨100⟩ in the {110} plane. We suppose that the nearly spherical Fermi surface of the a branch possesses large diameter arms centered in the ⟨111⟩ direction and at 23° from ⟨100⟩ in {110} plane. The b, b', b'' branches with a center at the ⟨111⟩ direction may be related to the arms. The carrier concentration of the nearly spherical a branch roughly corresponds to that of one ellipsoid in the paramagnetic state. As the carrier concentration does not change below the Néel temperature, the arms in the a branch and other Fermi surfaces may compensate the carrier concentration contributed by the remaining two ellipsoids.

In NdB_6 the signal of the a branch, the highest frequency in the antiferromagnetic state, disappears in the angular region of 40–90° in the {110} plane, and in a narrow angular range of approximately 1° centered at ⟨110⟩ in the {100} plane. This branch is approximately the same in area as the a branch in PrB_6, but the angular ranges over which it disappears are different, suggesting that its topology is different from PrB_6. Of the other branches, g and h have the strongest signals and are observed at all angles, suggesting that they arise from a nearly spherical closed sheet. The other orbits exist in finite angular ranges centered at ⟨111⟩, ⟨110⟩, or ⟨100⟩, except for the b orbit which does not appear near a symmetry direction. This pattern of orbits is not similar to that observed in PrB_6, suggesting that the Fermi surface topology in the antiferromagnetic state of the two metals is not the same. This conclusion is consistent with the very different magnetic structure and unit cell in the two materials.

In the antiferromagnetic states of PrB_6 and NdB_6, the masses do not follow simple scaling laws. In both materials, the masses are rather heavy, as shown by the a orbits which have masses of $2.52m_0$ and $2.00m_0$, respectively. While these masses are large compared to the non-f LaB_6, they are not large compared to typical transition-

metal compounds where magnetism is observed. Therefore it is possible that the antiferromagnetic modifications to the Fermi-surface band structure of these metals involve mostly *d-sp* hybridization.

V. CONCLUSION

We have measured the electrical resistivity, Hall coefficient, magnetoresistance, and the de Haas–van Alphen effect of PrB_6 and NdB_6 to study their Fermi-surface properties. The experimental results are as follows:

(1) The Hall coefficient is temperature independent in the range 0.7 K to room temperature. The number of conduction electrons is approximately one per unit cell. This is consistent with the Fermi-surface model of LaB_6, where a set of three electron ellipsoids centered at X and connected by small necks in the X-X direction contain one electron per unit cell. Even below the Néel temperature, the carrier concentration as measured by the Hall effect does not change.

(2) The magnetoresistance shows that both substances are uncompensated metals where the carriers are electrons. Open orbits are found at many angles in the $\{100\}$ and $\{110\}$ planes, implying a multiply connected Fermi surface in PrB_6 and NdB_6. The $\langle 100 \rangle$ direction is a singular field direction in NdB_6 but not in PrB_6.

(3) In PrB_6 we have observed the antiferromagnetic Fermi surface reflecting the smaller magnetic Brillouin zone induced by the magnetic structure, as well as the paramagnetic Fermi surface which can be seen due to magnetic breakdown through the small antiferromagnetic gaps. The paramagnetic Fermi surface consists of three ellipsoids which are the same as those of LaB_6. The necks interconnecting between ellipsoids are, however, larger than those of LaB_6, which removes the singular field direction at $\langle 100 \rangle$. The main antiferromagnetic Fermi surface is a nearly spherical Fermi surface with arms along the $\langle 111 \rangle$ directions.

(4) In NdB_6, only the antiferromagnetic Fermi surface has been observed, which is highly different from those of PrB_6 and LaB_6. The main Fermi surface is a nearly spherical sheet which is not observed over the whole angular range.

(5) The cyclotron mass of the paramagnetic main Fermi surface (ellipsoid) in PrB_6, $1.95m_0$, is three times larger than that of LaB_6, $0.61-0.64m_0$.

(6) The cyclotron masses of the antiferromagnetic dominant nearly spherical Fermi surfaces in PrB_6 and NdB_6 are $2.52m_0$ and $2.00m_0$, respectively. Although these masses are slightly heavier than those in the paramagnetic state, they are similar to those observed in other magnetic d-electron metals.

ACKNOWLEDGMENTS

We are grateful to B. I. Min, M. R. Norman, D. D. Koelling, Y. Ishizawa, and A. Hasegawa for their helpful discussions. This work was supported by the U.S. Department of Energy, Basic Energy Science–Materials Sciences under Contract No. W-31-ENG-38 and also by a Grant-In-Aid for Scientific Research from the Ministry of Education, Science, and Culture in Japan. One of us (A.U.) acknowledges support from the Natural Science and Engineering Council of Canada.

*Permanent address: Institute of Material Science, University of Tsukuba, Sakura-mura, Ibaraki 305, Japan.

†Also at University of Alberta, Edmonton, Alberta, Canada T6G 2J1.

‡Also at Purdue University, W. Lafayette, IN 47907.

[1]T. Kasuya, *Theory of Heavy Fermion and Valence Fluctuations,* edited by T. Kasuya and T. Saso (Springer-Verlag, Berlin, 1985), p. 2.

[2]D. D. Koelling, B. D. Dunlap, and G. W. Crabtree, Phys. Rev. B **31**, 4966 (1985).

[3]G. W. Crabtree, J. Magn. Magn. Mater. **52**, 169 (1985).

[4]T. Komatsubara, N. Sato, S. Kunii, I. Oguro, Y. Furukawa, Y. Onuki, and T. Kasuya, J. Magn. Magn. Mater. **31-34**, 368 (1983).

[5]S. Horn, F. Steglich, M. Loewenhaupt, H. Scheuer, W. Felsch, and K. Winzer, Z. Phys. B **42**, 125 (1981).

[6]C. M. McCarthy, C. W. Thompson, R. J. Graves, H. W. White, Z. Fisk, and H. R. Ott, Solid State Commun. **36**, 861 (1980).

[7]C. M. McCarthy and C. W. Thompson, J. Phys. Chem. Solids **41**, 1319 (1980).

[8]G. W. Crabtree, H. Aoki, W. Joss, and F. Hulliger, *Theoretical and Experimental Aspects of Valence Fluctuations and Heavy Fermions,* edited by L. C. Gupta and S. K. Malik (Plenum, New York, 1987). p. 197.

[9]W. R. Johanson, G. W. Crabtree, A. S. Edelstein, and O. D. McMasters, J. Magn. Magn. Mater. **31-34**, 377 (1983); W. R. Johanson, G. W. Crabtree, A. S. Edelstein, and O. D. McMasters, Phys. Rev. Lett. **46**, 504 (1981); G. W. Crabtree, W. R. Johanson, A. S. Edelstein, and O. D. McMasters, in *Valence Fluctuations in Solids,* edited by L. M. Falicov, W. Hanke, and M. B. Maple (North-Holland, Amsterdam, 1981), p. 93.

[10]P. H. P. Reinders, M. Springford, P. T. Coleridge, R. Boulet, and D. Ravot, Phys. Rev. Lett. **57**, 1631 (1986).

[11]L. Taillefer, R. Newbury, G. G. Lonzarich, Z. Fisk, and J. L. Smith, J. Magn. Magn. Mater. **63-64**, 372 (1987).

[12]A. J. Arko, G. W. Crabtree, D. Karim, F. M. Mueller, L. R. Windmiller, J. B. Ketterson, and Z. Fisk, Phys. Rev. B **13**, 5240 (1976).

[13]A. J. Arko, G. Crabtree, J. B. Ketterson, F. M. Mueller, P. F. Walch, L. R. Windmiller, Z. Fisk, R. Hoyt, A. Mota, R. Viswanathan, D. E. Ellis, A. J. Freeman, and J. Roth, Int. J. Quantum. Chem. Symp. **9**, 569 (1975).

[14]Y. Ishizawa, T. Tanaka, E. Bannai, and S. Kawai, J. Phys. Soc. Jpn. **42**, 112 (1977).

[15]Y. Ishizawa, H. Nozaki, T. Tanaka, and T. Nakajima, J. Phys. Soc. Jpn. **48**, 1439 (1980).

[16]P. F. Walch, D. E. Ellis, and F. M. Mueller, Phys. Rev. B **15**, 1859 (1977).

[17]A. Hasegawa and A. Yanase, J. Phys. F **2**, 1245 (1977).

[18]A. P. J. van Deursen, Z. Fisk, and A. R. de Vrooman, Solid State Commun. **44**, 609 (1982).

[19]A. P. J. van Deursen, R. E. Pols, A. R. de Vrooman, and Z. Fisk, J. Less-Common Met. **111**, 331 (1985).

[20]Y. Onuki, M. Nishihara, M. Sato, and T. Komatsubara, J. Magn. Magn. Mater. **52**, 317 (1985).
[21]N. Sato, A. Sumiyama, S. Kunii, H. Nagano, and T. Kasuya, J. Phys. Soc. Jpn. **54**, 1923 (1985).
[22]N. Sato, S. Kunii, I. Oguro, T. Komatsubara, and T. Kasuya, J. Phys. Soc. Jpn. **53**, 3967 (1984).
[23]T. Tanaka, E. Bannai, S. Kawai, and T. Yamani, J. Cryst. Growth **30**, 193 (1975).
[24]Y. Ishizawa *et al.*, Research Report of National Institute for Research in Inorganic Materials, Tsukuba, Japan, No. 17 (1978) (in Japanese) (unpublished).
[25]N. Sato, Ph.D. thesis, Tohoku University, 1983 (unpublished).
[26]S. Tanigawa, S. Terakado, Y. Iwase, R. Suzuki, T. Komatsubara, and Y. Onuki, J. Magn. Magn. Mater. **52**, (1985) 313.